



## PAPER

[View Article Online](#)  
[View Journal](#) | [View Issue](#)Cite this: *Catal. Sci. Technol.*, 2020,  
10, 6694Covalent structured catalytic materials containing  
single-atom metal sites with controllable spatial  
and chemical properties: concept and application†Ilse M. Denekamp, <sup>a</sup> Connor Deacon-Price, <sup>a</sup>  
Zhenhua Zhang, <sup>b</sup> and Gadi Rothenberg, <sup>\*a</sup>

We report a simple and scalable concept for designing a family of covalently-bound materials wherein single-atom metal sites are dispersed with a high degree of spatial and chemical control. Our method is based on a “ring and linker” building block combination, with highly stable phthalocyanine macrocycles connected by a variety of linkers using amide bonds. This approach enables the design of solid materials with precise distances between the single-atom sites. It is also versatile, allowing for diverse combinations via “mix & match” options. We demonstrate the concept in the synthesis of nine different copper- or cobalt-containing polymers, as well as their application in the selective oxygen reduction reaction. Our results show a clear relation between linker length and activity, demonstrating the power of this simple synthetic approach.

Received 29th June 2020,  
Accepted 19th August 2020

DOI: 10.1039/d0cy01299h

[rsc.li/catalysis](http://rsc.li/catalysis)

Designing catalysts for specific applications requires spatial and chemical control. We see this in natural systems, where enzymes catalyse reactions that we chemists can only dream of with envy.<sup>1</sup> Many of these enzymes rely on single-atom sites.<sup>2</sup> Some, such as methane monooxygenase, go further, and combine two metal atoms in a bifunctional site.<sup>3</sup> The superb spatial and chemical control enables these enzymes to carry out selective transformations under very mild conditions – something that we cannot do *in vitro*. Yet even if we cannot exactly mimic the enzymatic conditions, we can still adapt concepts and pieces of the natural puzzle for designing new active materials.<sup>4–6</sup> Moreover, chemistry allows us to “mix & match” these concepts and properties, creating solid materials that can function under harsh industrial conditions: high temperatures, pressures, and corrosive environments. In this way, we can adapt nature's concepts to our needs.<sup>7</sup>

This is especially true for oxygen activation<sup>8,9</sup> and for oxidative transformations,<sup>10</sup> where selectivity and stability

are a must. Here, nature typically uses the haem function, comprising a porphyrin macrocycle ligand with nitrogen atoms surrounding a single central metal atom. The active site is extremely well-defined, but the system is delicate, requiring a cumbersome protective protein shell. Ideally, we want to combine the specificity of the haem complex with the stability and functional flexibility of modern-day industrial materials. We want a stable material that can activate oxygen under a range of conditions, with highly defined monoatomic or diatomic sites.<sup>11,12</sup> Even more importantly, we want a flexible solution, where we can easily change the type of metal site, the distance between sites, and the properties of the surrounding environment. Last, but not least, the material must be scalable and affordable, so that it can be used in real-life applications.<sup>13,14</sup>

In this paper, we present the concept and application of such designable materials, using a covalent building-block and linker approach. We use functionalised phthalocyanines (Pcs) as stable synthetic porphyrin mimics, connecting these with a series of linkers into a solid network of well-defined single-atom sites. This approach is highly effective, giving full spatial and chemical control. By using phthalocyanines instead of porphyrins, we create materials with high thermal, chemical and mechanical stability.<sup>15</sup> Moreover, by “mixing” the phthalocyanine metal centres and linker lengths and types, we control both the distance between the metal sites and their surrounding environment. The effects of this control are demonstrated using the oxygen reduction reaction (ORR) as a case study.

<sup>a</sup> Van't Hoff Institute for Molecular Science, University of Amsterdam, Science Park 904, Amsterdam, 1098 XH, The Netherlands.

E-mail: [g.rothenberg@uva.nl](mailto:g.rothenberg@uva.nl); Web: <http://hims.uva.nl/hcsc>

<sup>b</sup> Key Laboratory of the Ministry of Education for Advanced Catalysis Materials, Institute of Physical Chemistry, Zhejiang Normal University, Jinhua 321004, P.R. China

† Electronic supplementary information (ESI) available: Detailed experimental procedures for all compounds, FTIR spectra and Koutecký-Levich plots for all of the copper polymer catalysts, LSV curves for the cobalt polymer catalysts and Fourier-transform curves for the EXAFS measurements. See DOI: 10.1039/d0cy01299h



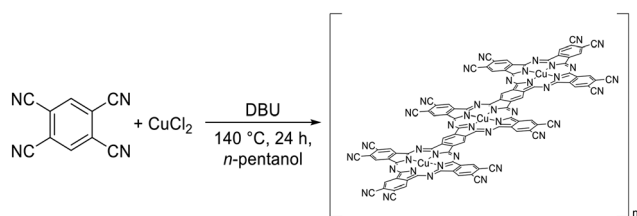
Single atom sites are excellent catalysts.<sup>16–21</sup> In the case of ORR, single metal- $N_x$  sites (where  $N_x$  denotes a complex with  $x$  nitrogen atoms ligating to the metal) achieve high activities.<sup>22–24</sup> We chose to focus on metal-phthalocyanine (MPc,  $N_4$  site) as active sites in ORR, since these give excellent activity.<sup>25,26</sup> Our hypothesis was that by carefully controlling the distances between the active sites we can influence the ORR activity, *e.g.* through confinement effects.<sup>27–29</sup>

Our concept is based on MPc complex building blocks, the rings of which are modified with connecting groups. These are linked to each other, either directly or using various organic linkers. The result is a solid material with well-defined single-atom sites connected by strong covalent bonds. Our synthetic approach combines the advantages of the phthalocyanine macrocycles as ligands with simple solid catalyst separation by filtration, while at the same time avoiding the problem of  $\pi$ -stacking.

We started by examining the possibility of linking the MPcs directly to each other. This can be done by polymerising the “double phthalonitrile” 1,2,4,5-tetracyanobenzene (Scheme 1).

Building on the classic procedure,<sup>30,31</sup> we optimised the protocol using *n*-pentanol as solvent, with copper(II) chloride and a strong base, 1,8-diazabicyclo[5.4.0]undec-7-ene (DBU).<sup>32</sup> The resulting dark green powder was characterised by Fourier-transform infrared spectroscopy (FTIR) and MALDI-TOF (characterisation details for all materials are included in the ESI†). However, this route still has two major drawbacks. First, it gives a high degree of polydispersity, due to multiple points of initiation. This also increases branching, resulting in an unpredictable polymer structure. Second, the batch reproducibility is poor, because the polymerisation depends strongly on local conditions. Thus, this direct route is inherently unsuitable for making designed materials.

To overcome these issues, we turned to a sequential approach. In this step-by-step synthesis we first add the substituted Pc building block to the linker in a 1 : 4 ratio (see Fig. 1; full experimental details are included in the ESI†). The building blocks react with the linkers *via* the coupling of acyl chlorides and amines, forming a nylon-type bond. This reaction is quick and efficient, giving near-quantitative yields under ambient atmosphere and 50 °C. After the Pc-linker node forms, four more equivalents of Pc are added, followed by 12 equivalents of linker, and so on. In this way, we grow the polymer as an expanding flat structure.



**Scheme 1** The synthesis of the directly linked  $\text{CuPcC}_6$  starting from 1,2,4,5-tetracyanobenzene and copper chloride.

This step-by-step addition gives a polymer of known size and weight. It also allows the design of specific polymers, by varying the metals used in the Pc, the linker size, or the linker type. This feature is extremely important, because it holds the key to spatial and chemical control. You can create well-defined, complex polymers where you choose the metals in the different rings, as well as the flexibility and distance between the rings (because you can use different linkers in different steps). Here we used four different linkers (Fig. 1): oxalyl chloride ( $\text{C}_2$ ), adipoyl chloride ( $\text{C}_6$ ), terephthaloyl chloride ( $\text{C}_{\text{TPA}}$ ) and sebacoyl chloride ( $\text{C}_{10}$ ).

Oxalyl chloride ( $\text{C}_2$ ) is the shortest linker, containing only two carbon atoms. Once linked, it is essentially two connected and conjugated amide bonds, with an inter-metal distance of approximately 18 Å, and a linker distance of 6 Å. This may allow for easier electron transfer across the metal sites. Adipoyl chloride ( $\text{C}_6$ ) is longer, approximately 10 Å, which increases the inter-metal distance to 23 Å. This linker is unconjugated and flexible. Its counterpart, terephthaloyl chloride ( $\text{C}_{\text{TPA}}$ ), features the same linker and inter-metal distances, yet is conjugated and rigid. Comparing  $\text{C}_6$  and  $\text{C}_{\text{TPA}}$  can help us quantify the effects of conjugation on the catalytic performance. Finally, sebacoyl chloride ( $\text{C}_{10}$ ) is even longer, with a linker size of 15 Å, and a nominal inter-metal distance of 27 Å. In practice, the distances may be smaller, as such large flexible linkers may promote folding and stacking. By choosing these four different linkers, we can compare the effects of length and flexibility on the materials' performance.

First, we synthesised the monomer building block,  $\text{MPc}(\text{NH}_2)_4$  (where M is either void, Co or Cu), by tetramerization of 4-aminophthalonitrile.<sup>32</sup> In the absence of metal (M = void) this gives the 2,9,16,23-tetra(amino) phthalocyanine,  $\text{H}_2\text{Pc}(\text{NH}_2)_4$ . The same procedure can be used for making  $\text{CuPc}(\text{NH}_2)_4$  or  $\text{CoPc}(\text{NH}_2)_4$ , by adding a copper or cobalt salt, respectively. These new compounds were characterised by high-resolution mass spectrometry (HRMS) and FTIR. Fig. 2 shows one peak at *ca.* 426  $\text{cm}^{-1}$ , attributed to the in-plane C–C–H bend, another at *ca.* 735  $\text{cm}^{-1}$  pertaining to the N–C–N inner ring “breathing”. Further, we see the C–H in-plane bend at *ca.* 1095  $\text{cm}^{-1}$  (1106  $\text{cm}^{-1}$  for  $\text{H}_2\text{Pc}(\text{NH}_2)_4$ ), the C–N stretch at *ca.* 1500  $\text{cm}^{-1}$  and the C=C macrocycle ring deformation at *ca.* 1593  $\text{cm}^{-1}$ . Additional characterisation details are included in the ESI†.

With the monomer and linkers at hand, we synthesised nine different copper-containing and cobalt-containing polymers. Table 1 gives the designation codes and the key synthesis and structure parameters for each polymer. For example, in entry 3,  $\text{CuPcC}_6$ , Cu is the metal atom; Pc indicates phthalocyanine and  $\text{C}_6$  denotes the linker (in this case, adipoyl chloride). Except for the linker-free direct-coupled sample, all of the polymers are based on three node rings connected by two sets of linkers (see Fig. 1, right-hand structure).

The disadvantage of such highly stable high-molecular-weight covalent polymers is that their analysis is extremely



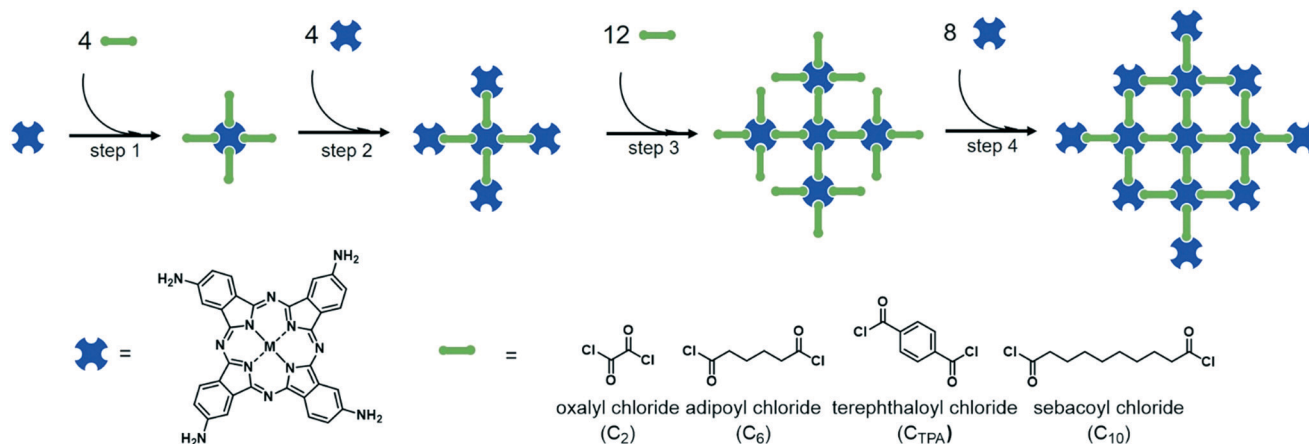


**Fig. 1** The synthesis of the polymers. Blue building blocks represent the  $\text{MPC}(\text{NH}_2)_4$  and green linkers denote oxalyl chloride ( $\text{C}_2$ ), adipoyl chloride ( $\text{C}_6$ ), terephthaloyl chloride ( $\text{C}_{\text{TPA}}$ ) and sebacoyl chloride ( $\text{C}_{10}$ ). All polymers in this paper were prepared by this four-step synthesis, with the exception of the  $\text{CuPcC}_0$  which was made following the route shown in Scheme 1.

challenging. They are practically insoluble, regardless of solvent and conditions, precluding SEC and HRMS analysis (we did succeed in HRMS analysis of the smallest structure). For the  $\text{CuPcC}_0$  we saw at least three MPCs connected to each other, after which the data becomes too noisy. They are also amorphous, ruling out X-ray diffraction. Moreover, as carbonaceous molecular species, they are too small and too transparent for microscopy analysis (we ran detailed SPM, SEM and TEM studies with no results). Three methods, however, are possible: elemental analysis, vibrational spectroscopy (FTIR) and X-ray absorption spectroscopy (XAS).

Elemental analysis is the most reliable quantitative method for determining the composition of samples. Analysis of  $\text{CuPcC}_2$  and  $\text{CuPcC}_{10}$  showed that each polymer containing 13 rings and 16 linkers (right-hand structure in Fig. 1), showed that their elemental compositions fit well with the calculated values (calcd. for  $\text{CuPcC}_2$ : C: 58.9, H: 2.5, N: 23.9, Cu: 9.1 wt%; found: C: 58.9, H: 3.4, N: 22.8, Cu: 9.2 wt%; calcd. for  $\text{CuPcC}_{10}$ : C: 63.3, H: 4.5, N: 20.0, Cu: 7.6; found: C: 61.9, H: 5.9, N: 19.7, Cu: 7.6; see ESI† for details). Both samples contained <0.1 wt% of Cl, confirming that the reaction of the linkers was near-quantitative.

The FTIR spectra of  $\text{CuPcC}_{\text{TPA}}$  and  $\text{CuPcC}_0$  in Fig. 2 show that the overall profiles of the polymers are very similar. The

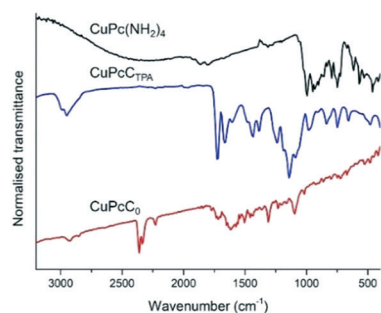


**Fig. 2** FTIR of  $\text{CuPc}(\text{NH}_2)_4$  (black)  $\text{CuPcC}_{\text{TPA}}$  (blue) and  $\text{CuPcC}_0$  (red).

strong peak at  $1650\text{ cm}^{-1}$  indicates a  $\text{C}=\text{O}$  stretch vibration of the secondary amide. This peak confirms the polymerisation (*cf.* the spectrum of the pristine monomer building block). The same conclusion can be drawn from the peak at  $2920\text{ cm}^{-1}$ , showing the alkane C–H stretch. All of the other C–H bonds are aromatic, pertaining to the Pc rings.

The X-ray absorption spectra (XAS) of  $\text{CuPc}(\text{NH}_2)_4$  and  $\text{CuPcC}_{\text{TPA}}$  are highly similar (Fig. 3), suggesting that the copper centres in both materials are identical. CuPc has a  $\text{Cu}^{2+}$  metal centre, indicated by the pre-edge feature and the absorption edge positions.<sup>33,34</sup> The radial distribution indicates that the distance from Cu to its nearest neighbour is  $1.5\text{ \AA}$  (see details in the ESI†), confirming the C–N dative bond.<sup>33</sup> The large distance ( $>20\text{ \AA}$ ) between the copper atoms even in the smallest CuPc polymer precludes the detection of any Cu–Cu interaction in the EXAFS region. The inset in Fig. 3 shows the residuals plot of the EXAFS data. The data itself is smoothed, but all the removed data is shown in the residuals plot. This plot shows a random scatter, confirming that no meaningful information was lost in the smoothing process.

Another experimental technique that combines analysis and performance studies is ORR. Here we follow the reduction of oxygen to water, typically *via* the four-electron route (Scheme 2). This reaction can happen in three ways: the first is the reduction of oxygen to hydrogen peroxide which is adsorbed on the surface, after which it is further reduced to water (or, in our basic environment, to  $\text{OH}^-$ ).<sup>35</sup> The second pathway begins similarly with the reduction of oxygen to hydrogen peroxide, which then desorbs from the surface and is ultimately reduced to  $\text{OH}^-$  in the bulk solution.<sup>36,37</sup> Finally, there is also the (undesired) two-electron reduction of oxygen to hydrogen peroxide as final product.

The mechanism of ORR on Pcs was studied by Chen *et al.*<sup>38</sup> and by Nørskov and co-workers.<sup>39</sup> In brief, oxygen binds with one oxygen atom to the metal and the other



**Table 1** Designation and parameters of the Pc polymers

| Entry | Polymer              | Linker     |             | Diameter <sup>a</sup><br>(Å) | mw <sup>b</sup><br>(kDa) |
|-------|----------------------|------------|-------------|------------------------------|--------------------------|
|       |                      | Length (Å) | Conjugation |                              |                          |
| 1     | CuPcC <sub>0</sub>   | —          | —           | Unknown                      | Unknown                  |
| 2     | CuPcC <sub>2</sub>   | 6          | ✓           | 84                           | 9.1                      |
| 3     | CuPcC <sub>6</sub>   | 10         | ✗           | 104                          | 10.0                     |
| 4     | CuPcC <sub>TPA</sub> | 10         | ✓           | 104                          | 10.4                     |
| 5     | CuPcC <sub>10</sub>  | 15         | ✗           | 120                          | 10.9                     |
| 6     | CoPcC <sub>2</sub>   | 6          | ✓           | 84                           | 9.1                      |
| 7     | CoPcC <sub>6</sub>   | 10         | ✗           | 104                          | 10.0                     |
| 8     | CoPcC <sub>TPA</sub> | 10         | ✓           | 104                          | 10.3                     |
| 9     | CoPcC <sub>10</sub>  | 15         | ✗           | 120                          | 10.9                     |

<sup>a</sup> Nominal diameter based on a flat symmetric structure. <sup>b</sup> Theoretical mw of the polymer based on three node rings connected by two sets of linkers.

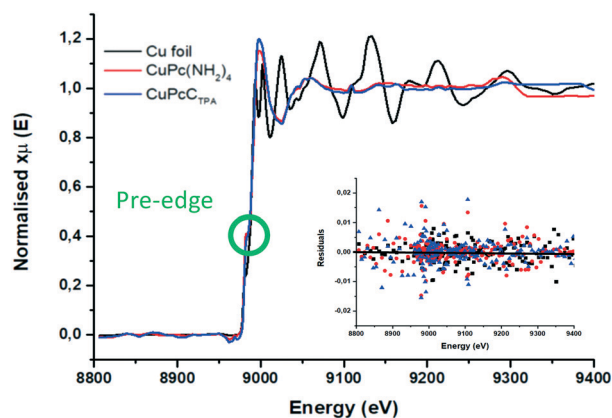
oxygen will position itself between two nitrogen atoms of the Pc.<sup>38</sup> Oxygen adsorption is the key step in controlling the ORR onset potential in a basic environment. After the adsorption of O<sub>2</sub>, it can react in two ways. It can react with one proton and electron from the surrounding water to form the active OOH<sup>−</sup>, or dissociate; leaving the surface as an unreacted molecule. After a proton transfer, the OH<sup>−</sup> in the surrounding O<sub>2</sub>, dissociation becomes more facile, since water at the surface is a stronger proton donor than OH<sup>−</sup>.<sup>36,39</sup> Clustering of the copper atom centres is unlikely, since Pcs are stable at high pressure and temperature. Moreover, were clustering to occur, all the LSV curves would be the same, because the metal distance is the only difference between the polymers. This is not the case, hence the copper atoms do not cluster.

Prior to reaction, we supported the Pc and polymerised Pc samples on activated carbon to increase their conductivity and adhesion to the electrode surface. The ORR activity was measured with linear sweep voltammetry (LSV) in a 0.1 M KOH electrolyte, degassed with O<sub>2</sub> and using a scan rate of 10 mV s<sup>−1</sup>. Control experiments confirmed that unsupported monomer samples and metal-free monomers have little or no activity (Fig. 4). Of the two supported monomers, the

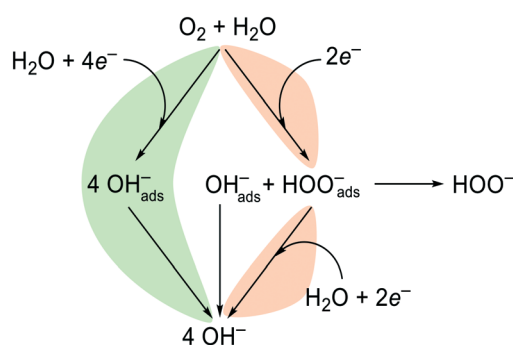
CoPcH<sub>16</sub> outperformed its copper counterpart, giving a lower onset potential. However, in the following example we present the copper-containing samples, as the differences between the different linker combinations are easier to see and analyse (the full data for the cobalt-containing samples is included in the ESI†). Both CoPcH<sub>16</sub> and CuPcH<sub>16</sub> are stable under these oxidative conditions, as shown also elsewhere.<sup>40</sup>

Fig. 5 shows the linear sweep voltammetry curves of the polymer CuPc set. Shorter linkers give lower onset potentials. This may reflect the effect of the inter-metal distance. When the metal ions are closer to each other, the ORR activity increases. This effect is observed both for cobalt and copper. The monomer CuPc (dashed curve in Fig. 5) shows an onset potential similar to that of the polymers with intermediate linker sizes. However, the factors affecting the performance of the monomer catalysts are more complex. The MPc monomers can stack on the surface, resulting in many possible interactions between them.

We can explain the influence of the inter-metal distance on the ORR performance if we consider the solvation shell. The metal ions can polarise the water molecules to accommodate charges on the surface.<sup>41</sup> This creates a different environment in the immediate vicinity of the copper



**Fig. 3** EXAFS data at the Cu K edge for Cu foil (black), CuPc(NH<sub>2</sub>)<sub>4</sub> (red) and CuPcC<sub>TPA</sub> (blue). The green circle shows the pre-edge position. The inset shows the residuals plot, which is unstructured.



**Scheme 2** The oxygen reduction reaction can proceed via either the direct four-electron route (green) or the indirect 2 + 2 electron route (orange). In the latter case, the reaction can also stop after the first step, giving one hydroxyl ion and one hydroperoxyl ion.





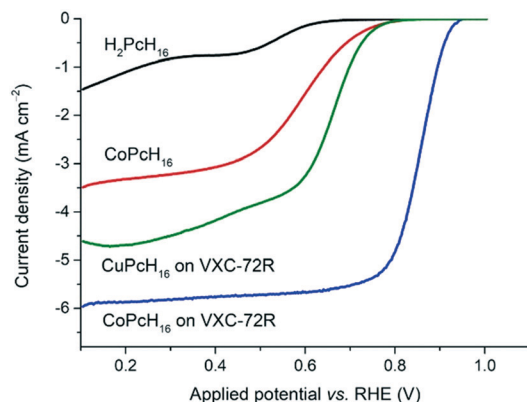


Fig. 4 LSV curve of different monomer Pcs obtained in 0.1 M KOH, degassed with  $O_2$ , a scan rate of  $10 \text{ mV s}^{-1}$  and a rotation speed of 1600 rpm. Shown is  $H_2PcH_{16}$  (black),  $CoPcH_{16}$  (red)  $CuPcH_{16}$  supported on VXC-72R (green) and  $CoPcH_{16}$  supported on VXC-72R (blue).

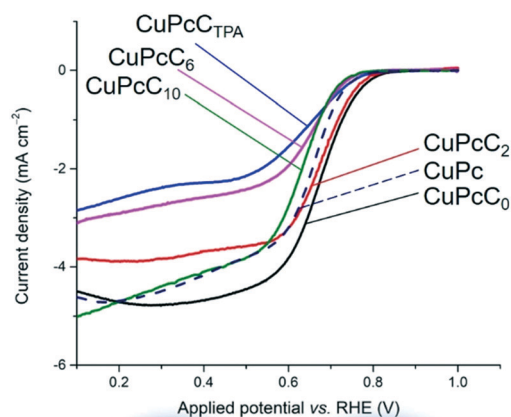


Fig. 5 Top: LSV curves of  $CuPcC_0$  (black),  $CuPcC_2$  (red)  $CuPcC_6$  (pink),  $CuPcC_{TPA}$  (blue),  $CuPcC_{10}$  (green) and monomer  $CuPc$  (dashed blue) obtained in 0.1 M KOH, degassed with  $O_2$ , a scan rate of  $10 \text{ mV s}^{-1}$  and a rotation speed of 1600 rpm. Bottom: Illustration of two adjacent  $CuPcs$  with overlapping solvation shells.

(or cobalt) Pcs. The “thickness” of this shell is typically 2–3 molecular layers (4–5 Å). When two Pcs are within the distance of influence, their solvation shells will partially

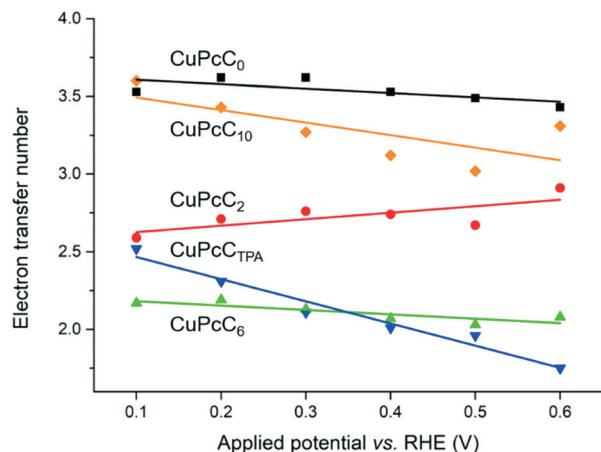


Fig. 6 Data obtained from the Koutecký-Levich analysis, showing the electron transfer number of each polymer at a certain potential. Shown is  $CuPcC_0$  (black),  $CuPcC_2$  (red)  $CuPcC_6$  (green),  $CuPcC_{TPA}$  (blue),  $CuPcC_{10}$  (orange).

overlap (see Fig. 5, bottom), increasing the likelihood of the four-electron route. This holds true for the  $C_0$  and  $C_2$  linkers, but doesn't apply to the longer ones, explaining the difference in ORR activity.

Table 2 compares the onset potentials (V vs. RHE) of our five polymer Pcs to those of Pt/C, CuO/C and CuPc benchmark materials, as well as analogous polymers. The ORR performance of our polymers is good, but not exceptional. However, we are not screening here for an optimised ORR catalyst. Rather, we are showing that this synthesis method gives easy access to covalent materials with good spatial and chemical control.

The ORR activity strongly depends on the inter-metal distance, yet the product selectivity shows a different trend. Koutecký-Levich analysis (Fig. 6) shows that the middle-sized linkers give the hydrogen peroxide product (top section of the orange route in Scheme 2 above). Conversely, catalysts with no linker ( $C_0$ ) or with long linkers ( $C_{10}$ ) are selective towards the  $OH^-$  product (green route in Scheme 2). A detailed mechanistic study using RRDE is out of the scope of this paper,<sup>42–44</sup> but it is likely that the two extreme cases (short vs. long linkers) are influenced by different factors (*cf.* the mass-transfer barrier observed for the polymer with the  $C_{10}$  linker in Fig. 5, which is not observed for the short linkers).

Table 2 Onset potentials of Pc polymers and related benchmarks

| Entry | Material                           | Onset potential (V vs. RHE) | Entry | Material      | Onset potential (V vs. RHE) |
|-------|------------------------------------|-----------------------------|-------|---------------|-----------------------------|
| 1     | Pt/C                               | 0.94                        | 5     | $CuPcC_0$     | 0.81                        |
| 2     | CuO/C                              | 0.77                        | 6     | $CuPcC_2$     | 0.80                        |
| 3     | $CuPcH_{16}/C$                     | 0.73                        | 7     | $CuPcC_6$     | 0.76                        |
| 4     | Yasuda <i>et al.</i> <sup>25</sup> | 0.97                        | 8     | $CuPcC_{TPA}$ | 0.77                        |
| 5     | Liu <i>et al.</i> <sup>26</sup>    | 0.99                        | 9     | $CuPcC_{10}$  | 0.75                        |

The onset potential is shown at a current density of  $100 \mu\text{A cm}^{-2}$ . All materials are supported on carbon VXC-72R (C). The Pt loading is 20 wt%.



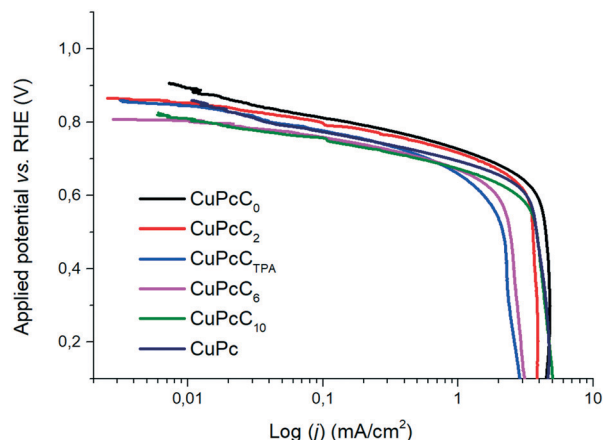


Fig. 7 Tafel plot of the CuPcC<sub>0</sub> (black), CuPcC<sub>2</sub> (red), CuPcC<sub>TPA</sub> (blue), CuPcC<sub>6</sub> (pink), CuPcC<sub>10</sub> (green) and CuPcH<sub>16</sub> (navy) obtained in 0.1 M KOH, degassed with O<sub>2</sub>, at a scan rate of 10 mV s<sup>-1</sup> and a rotation speed of 1600 rpm.

The slope of the Tafel plot (Fig. 7) gives information about the rate-determining step (RDS). If this slope is around 120 mV dec<sup>-1</sup>, the RDS is an electron transfer. If not, it is an adsorption or desorption of species, such as the adsorption of oxygen or the desorption of OH<sup>-</sup> or OOH<sup>-</sup>.<sup>45,46</sup> The RDS can change according to the applied current or potential. Thus, we studied both the low current density (LCD) and high current density (HCD) to monitor these changes in the RDS. In our case, the LCD shows a slope between 60 and 70 mV dec<sup>-1</sup>, indicating an adsorption or desorption in the RDS. In the HCD the slope is between 100 and 120 mV dec<sup>-1</sup>, indicating partly adsorption or desorption, and an electron transfer as RDS (see ESI† for the exact numbers). This could be an adsorbed OH<sup>-</sup> species that desorbs to give OH<sup>-</sup> in solution or adsorbed O<sub>2</sub> undergoes an electron transfer and becomes adsorbed OOH<sup>-</sup>, which is the first step of ORR.

In conclusion, the “ring and linker” method presented here is a scalable and structured approach for preparing covalently-bound macrocyclic polymer solids with well-defined single-atom sites. This method allows for excellent spatial and chemical control, while benefitting from the strength and stability of covalent bonding. The resulting polymers are good ORR catalysts. Moreover, the generality of our method opens opportunities for designing new types of catalysts and performance materials.

## Conflicts of interest

There are no conflicts to declare.

## Acknowledgements

We thank E. Zuidinga for the HRMS measurements, Prof. V. Gitis (Ben-Gurion University) for help with AFM, SPM, XPS and HRTEM measurements, Prof. W. Huang (USTC Hefei) for making the contact for the XAS measurements and T. K. Slot for help with the XAS data analysis. I. M. D. is supported by

the NWO TOP-PUNT project Catalysis in Confined Spaces (project 718.015.004). This work is part of the Research Priority Area Sustainable Chemistry of the UvA, <http://suschem.uva.nl>.

## Notes and references

- X. Zheng, G. Shen, C. Wang, Y. Li, D. Dunphy, T. Hasan, C. J. Brinker and B.-L. Su, *Nat. Commun.*, 2017, **8**, 1–9.
- G. Vilé, D. Albani, M. Nachttegaal, Z. Chen, D. Dontsova, M. Antonietti, N. López and J. Pérez-Ramírez, *Angew. Chem., Int. Ed.*, 2015, **54**, 11265–11269.
- M. Merckx, D. A. Kopp, M. H. Sazinsky, J. L. Blazyk, J. Müller and S. J. Lippard, *Angew. Chem., Int. Ed.*, 2001, **40**, 2782–2807.
- Z. Guo, W. Liu and B. L. Su, *J. Colloid Interface Sci.*, 2011, **353**, 335–355.
- M. C. Gutiérrez, M. Jobbágy, N. Rapún, M. L. Ferrer and F. del Monte, *Adv. Mater.*, 2006, **18**, 1137–1140.
- Y. H. Deng, W. L. Yang, C. C. Wang and S. K. Fu, *Adv. Mater.*, 2003, **15**, 1729–1732.
- Y. Yao, X. Zeng, F. Wang, R. Sun, J. Xu and C.-P. Wong, *Chem. Mater.*, 2016, **28**, 1049–1057.
- K. Yamamoto, S. Tanaka, H. Hosoya, H. Tsurugi, K. Mashima and C. Copéret, *Helv. Chim. Acta*, 2018, **101**, e1800156.
- S. Shirase, K. Shinohara, H. Tsurugi and K. Mashima, *ACS Catal.*, 2018, **8**, 6939–6947.
- A. Abad, A. Corma and H. García, *Chem. – Eur. J.*, 2008, **14**, 212–222.
- F. R. Lucci, J. Liu, M. D. Marcinkowski, M. Yang, L. F. Allard, M. Flytzani-Stephanopoulos and E. C. H. Sykes, *Nat. Commun.*, 2015, **6**, 1–8.
- S. H. Lee, J. Kim, D. Y. Chung, J. M. Yoo, H. S. Lee, M. J. Kim, B. S. Mun, S. G. Kwon, Y.-E. Sung and T. Hyeon, *J. Am. Chem. Soc.*, 2019, **141**, 2035–2045.
- C. Coney, C. Hardacre, K. Morgan, N. Artioli, A. P. E. York, P. Millington, A. Kolpin and A. Goguet, *Appl. Catal., B*, 2019, **258**, 117918.
- C. J. Allen, J. Hwang, R. Kautz, S. Mukerjee, E. J. Plichta, M. A. Hendrickson and K. M. Abraham, *J. Phys. Chem. C*, 2012, **116**, 20755–20764.
- R. M. Ion, *Phthalocyanines Some Curr. Appl.*, InTech., 2017, DOI: 10.5772/intechopen.68654.
- Y. Qu, Z. Li, W. Chen, Y. Lin, T. Yuan, Z. Yang, C. Zhao, J. Wang, C. Zhao, X. Wang, F. Zhou, Z. Zhuang, Y. Wu and Y. Li, *Nat. Catal.*, 2018, **1**, 781–786.
- J. Li, Y. Li and T. Zhang, *Sci. China Mater.*, 2020, **63**, 889–891.
- F. Schüth, *Angew. Chem., Int. Ed.*, 2014, **53**, 8599–8604.
- S. Liang, C. Hao and Y. Shi, *ChemCatChem*, 2015, **7**, 2559–2567.
- J. M. Thomas, R. Raja and D. W. Lewis, *Angew. Chem., Int. Ed.*, 2005, **44**, 6456–6482.
- M. Soorholtz, L. C. Jones, D. Samuelis, C. Weidenthaler, R. J. White, M.-M. Titirici, D. A. Cullen, T. Zimmermann, M. Antonietti, J. Maier, R. Palkovits, B. F. Chmelka and F. Schüth, *ACS Catal.*, 2016, **6**, 2332–2340.



- 22 P. Yin, T. Yao, Y. Wu, L. Zheng, Y. Lin, W. Liu, H. Ju, J. Zhu, X. Hong, Z. Deng, G. Zhou, S. Wei and Y. Li, *Angew. Chem.*, 2016, **128**, 10958–10963.
- 23 Z. Chen, S. Mitchell, E. Vorobyeva, R. K. Leary, R. Hauert, T. Furnival, Q. M. Ramasse, J. M. Thomas, P. A. Midgley, D. Dontsova, M. Antonietti, S. Pogodin, N. López and J. Pérez-Ramírez, *Adv. Funct. Mater.*, 2017, **27**, 1605785.
- 24 P. Peng, L. Shi, F. Huo, C. Mi, X. Wu, S. Zhang and Z. Xiang, *Sci. Adv.*, 2019, **5**, eaaw2322.
- 25 S. Yasuda, A. Furuya, Y. Uchibori, J. Kim and K. Murakoshi, *Adv. Funct. Mater.*, 2016, **26**, 738–744.
- 26 Y. Liu, Y.-Y. Wu, G.-J. Lv, T. Pu, X.-Q. He and L.-L. Cui, *Electrochim. Acta*, 2013, **112**, 269–278.
- 27 I. M. Denekamp, M. Antens, T. K. Slot and G. Rothenberg, *ChemCatChem*, 2018, **10**, 1035–1041.
- 28 P. Liu, V. Degirmenci and E. J. M. Hensen, *J. Catal.*, 2014, **313**, 80–91.
- 29 T. K. Slot, D. Eisenberg and G. Rothenberg, *ChemCatChem*, 2018, **10**, 2119–2124.
- 30 H. Vogel and C. S. Marvel, *J. Polym. Sci.*, 1961, **50**, 511–539.
- 31 D. I. Packham, J. D. Davies and H. M. Paisley, *Polymer*, 1969, **10**, 923–931.
- 32 I. M. Denekamp, F. L. P. Veenstra, P. Jungbacker and G. Rothenberg, *Appl. Organomet. Chem.*, 2019, **33**, e4872.
- 33 G. Rossi, F. d'Acapito, L. Amidani, F. Boscherini and M. Pedio, *Phys. Chem. Chem. Phys.*, 2016, **18**, 23686–23694.
- 34 J. Chaboy, A. Muñoz-Páez, F. Carrera, P. Merkling and E. S. Marcos, *Phys. Rev. B*, 2005, **71**, 134208.
- 35 Y. Li, B. Chen, X. Duan, S. Chen, D. Liu, K. Zang, R. Si, F. Lou, X. Wang, M. Rønning, L. Song, J. Luo and D. Chen, *Appl. Catal., B*, 2019, **249**, 306–315.
- 36 L. Yu, X. Pan, X. Cao, P. Hu and X. Bao, *J. Catal.*, 2011, **282**, 183–190.
- 37 O. Antoine, Y. Bultel and R. Durand, *J. Electroanal. Chem.*, 2001, **499**, 85–94.
- 38 R. Chen, H. Li, D. Chu and G. Wang, *J. Phys. Chem. C*, 2009, **113**, 20689–20697.
- 39 V. Tripković, E. Skúlason, S. Siahrostami, J. K. Nørskov and J. Rossmeisl, *Electrochim. Acta*, 2010, **55**, 7975–7981.
- 40 L. Cui, L. Cui, Z. Li, J. Zhang, H. Wang, S. Lu and Y. Xiang, *J. Mater. Chem. A*, 2019, **7**, 16690–16695.
- 41 M. F. Kropman and H. J. Bakker, *Science*, 2001, **291**, 2118–2120.
- 42 S. Zhao, X. Zhao, S. Ouyang and Y. Zhu, *Catal. Sci. Technol.*, 2018, **8**, 1686–1695.
- 43 Y. Cao, Y. Zhu, X. Chen, B. S. Abrahama, W. Peng, Y. Li, G. Zhang, F. Zhang and X. Fan, *Catal. Sci. Technol.*, 2019, **9**, 6606–6612.
- 44 S. Ghosh, P. Kar, N. Bhandary, S. Basu, S. Sardar, T. Maiyalagan, D. Majumdar, S. K. Bhattacharya, A. Bhaumik, P. Lemmens and S. K. Pal, *Catal. Sci. Technol.*, 2016, **6**, 1417–1429.
- 45 T. Shinagawa, A. T. Garcia-Esparza and K. Takanabe, *Sci. Rep.*, 2015, **5**, 13801.
- 46 Y. H. Fang and Z.-P. Liu, *ACS Catal.*, 2014, **4**, 4364–4376.

